Title

Aberrant Cell and Basement Membrane Architecture Contribute to Sidestream Smoke-Induced Choroidal Endothelial DysfunctionETS-Induced Choroidal Endothelial Dysfunction

Journal

Investigative Ophthalmology & Visual Science, 55(5)

ISSN

0146-0404

Authors

Yang, Xiao
Scott, Harry A
Ardekani, Soroush
et al.

Publication Date

2014-05-15

DOI

10.1167/iovs.13-13659

Peer reviewed

Aberrant Cell and Basement Membrane Architecture Contribute to Sidestream Smoke-Induced Choroidal Endothelial Dysfunction

Xiao Yang,[1] Harry A. Scott,[1] Soroush Ardekani,[1] Monique Williams,[2] Prue Talbot,[2,3] and Kaustabh Ghosh[1,3]

[1]Department of Bioengineering, University of California-Riverside, Riverside, California, United States
[2]Department of Cell Biology and Neuroscience, University of California-Riverside, Riverside, California, California, United States
[3]Stem Cell Center, University of California-Riverside, Riverside, California, California, United States

Correspondence: Kaustabh Ghosh, Department of Bioengineering, University of California-Riverside, Riverside, CA 92521, USA; kghosh@engr.ucr.edu.

Submitted: November 22, 2013
Accepted: March 30, 2014

Citation: Yang X, Scott HA, Ardekani S, Williams M, Talbot P, Ghosh K. Aberrant cell and basement membrane architecture contribute to sidestream smoke-induced choroidal endothelial dysfunction. *Invest Ophthalmol Vis Sci*. 2014;55:XXXX–XXXX. DOI: 10.1167/iovs.13-13659

Purpose. Environmental tobacco smoke (ETS) is widely regarded as a major modifiable risk factor for age-related macular degeneration (AMD). Yet, precisely how it exerts its pathologic effects is poorly understood. Since early-stage AMD is characterized by choroidal capillary loss, this study examined the effect of sidestream smoke (SS), the major component of ETS, on the viability of choroidal endothelial cells (EC), with an emphasis on the role of aberrant cell and basement membrane (BM) architecture in mediating SS-induced response.

Methods. Chorioretinal ECs (RF/6A) were treated with SS, and cell viability and architecture were analyzed by colorimetric assay and actin cytoskeletal organization, respectively. The structure of RF/6A EC-secreted BM was examined by immunofluorescence for collagen IV and immunoblotting for lysyl oxidase (LOX), a collagen-crosslinking enzyme. Finally, fresh RF/6A ECs were cultured on decellularized SS-treated BM to evaluate its active role in EC dysfunction.

Results. The RF/6A EC viability decreased progressively with increasing SS dose, which correlated strongly with a significant decline in actin cytoskeleton-dependent EC spreading. Sidestream smoke also caused marked disruption of the RF/6A EC-secreted BM that was accompanied by suppression of LOX expression. Further, fresh, non–SS-treated RF/6A ECs exhibited a significant loss in viability and actin cytoskeletal organization when cultured on SS-treated corrupt BM.

Conclusions. These findings indicate that aberrant physical cues in the form of EC and BM architecture likely have an important role in choriocapillaris dysfunction seen in SS-associated early AMD and implicate choroidal BM as a potential target for AMD management strategies.

Keywords: choroid, tobacco smoke, basement membrane, cytoskeleton, endothelial cells, AMD

Environmental tobacco smoke (ETS), composed predominantly of sidestream smoke (SS) that arises from the tip of a burning cigarette, is the most common and potent indoor air pollutant in the developed world. Environmental tobacco smoke is widely regarded as a major modifiable risk factor for various eye diseases including degenerative age-related macular degeneration (AMD), the leading cause of blindness in the Western world.[1,2] The early stage of AMD (dry AMD) is characterized by accumulation of cellular and extracellular debris (termed drusen) between the retinal pigment epithelium (RPE) and the choroid.[3] Dry AMD typically leads to partial vision loss that may progress to severe blindness. As the disease progresses, the choroidal vessels (choriocapillaris) multiply and become leaky, leading to macular edema and loss of central vision (wet AMD). Current AMD therapies aim to suppress these newly-formed aberrant vessels in the wet stage by inhibiting endothelial cell (EC) proliferation and capillary formation.[4,5] However, these treatments are applicable only to a small subset (10%–15%) of all AMD patients who develop wet AMD. Thus, there is a great need to understand and inhibit the processes that underlie the earlier stage of dry AMD.

Recent studies have shown that the development of drusen is characterized by defects in the choriocapillaris, the inner vascular layer of the choroid.[6–8] Specifically, the choriocapillaris density is lower in regions with greater drusen accumulation.[6,8] Importantly, this decrease in choriocapillaris density correlates with an increase in the number of "ghost" choroidal vessels that are devoid of ECs. Whether there is a causal relationship between drusen accumulation and aberrant choriocapillaris remains unknown. Nonetheless, the choroidal vascular insufficiency is expected to deprive the retinal tissue of oxygen and nutrients. This, in turn, will likely cause ischemia-mediated oxidative stress, which is an important determinant of RPE dysfunction in early-stage AMD.[9,10] Thus, rescuing the degenerating choriocapillaris at the earlier stage (dry form) may help prevent or delay AMD progression. However, success in this pursuit will require a deeper understanding of the mechanisms that govern choroidal endothelial function.

It is known that, in addition to soluble and genetic factors, the physical form of cells and the extracellular matrix (ECM) also actively regulate endothelial function and capillary formation.[11–14] This physical control of endothelial function is

mediated by a mechanical force balance between the contractile forces generated by the actin cytoskeleton and that resisted by cell–ECM and cell–cell adhesions. By the process of mechanotransduction, these microscale mechanical forces are subsequently transduced into intracellular biochemical signals that ultimately control gene transcription and cell behavior.[15,16] Importantly, alterations in actin cytoskeletal organization or ECM structure lead to EC dysfunction and vascular anomalies.[17–20] This raises the question: Does aberrant choroidal EC and basement membrane architecture contribute to the choriocapillaris defects seen during ETS-associated dry AMD? Understanding this mechanism may help identify new mechanotransduction-based molecular targets for choriocapillaris normalization and improved AMD therapies in the future.

Using in vitro studies, we here show that exposure to SS, the major component of ETS, significantly reduces choroidal EC viability, a key determinant of choriocapillaris form and function. This suppression of EC viability results, at least in part, from the collapse of endothelial basement membrane (BM) architecture that, in turn, feeds back to disrupt cell shape- and cytoskeleton-dependent cell viability. Our findings also implicate lysyl oxidase (LOX), a copper-dependent ECM-crosslinking enzyme,[21] as an important mediator of SS-induced BM disruption.

Materials and Methods

Tobacco Smoke Solution

Mainstream and sidestream tobacco smoke solutions were prepared using a University of Kentucky analytical smoking machine, as described previously.[22,23] Briefly, mainstream smoke (MS) solution was made by drawing two-second puffs of Marlboro Red (Phillip Morris, Richmond, VA, USA) cigarette smoke every minute through minimum essential medium (Life Technologies, Carlsbad, CA, USA) to produce solutions at a concentration of 2 puffs/mL. The SS solution (2 puffs/mL) was made by collecting the smoke from the burning end of the cigarette and passing it through minimum essential medium. Mainstream and sidestream smoke solutions were made at physiologic pH and filtered using a 0.22-μm Acrodisk filter (Fisher Scientific, Tustin, CA, USA) under sterile conditions. Since nicotine is a very commonly studied tobacco compound for evaluation of cigarette smoke toxicity,[24–26] liquid chromatography-tandem mass spectrometry was used to measure the nicotine concentration in SS solutions.

Cell Culture and Tobacco Treatment

Chorioretinal EC line (RF/6A) was purchased from ATCC (Manassas, VA, USA). Cells were cultured on tissue culture dishes and grown in Eagle's minimum essential medium (EMEM; ATCC) supplemented with 10% fetal bovine serum (FBS, Fisherbrand; Fisher Scientific) and ×1 antimycotic/antibiotic mixture (Life Technologies), as per the protocol of ATCC. To facilitate BM deposition by RF/6A ECs during the assays, ascorbic acid (200 μg/mL; Sigma-Aldrich, St. Louis, MO, USA) was added to the assay culture medium. Cells were subjected to smoke treatment as follows: the stock solution (2 puffs/mL) was diluted to the desired concentration (0, 0.062, 0.125, 0.25, or 0.5 puffs/mL) in growth medium supplemented with ascorbic acid (200 μg/mL) and added to confluent RF/6A EC monolayers. After 9 days of SS treatment, the growth medium was replaced with smoke-containing low serum (2% FBS) medium and cells were cultured overnight before the specific assay. Liquid chromatography-tandem mass spectrometry measurements revealed that the SS stock solution of 2 puffs/mL corresponded to a nicotine concentration of approximately 4.641 μg/mL. Thus, nicotine concentration in the final SS working doses were approximately 144.2 ng/mL (corresponding to 0.062 puffs/mL), 290.7 ng/mL (0.125 puffs/mL), and 581.4 ng/mL (0.25 puffs/mL). Thus, these in vitro nicotine levels in SS were within the range of nicotine found in tissues of passive smokers.

EC-Derived Basement Membrane

To obtain cell-free endothelial BM, RF/6A ECs were cultured on glass cover slips coated with glutaraldehyde-crosslinked gelatin, as reported previously.[27,28] Briefly, autoclaved glass coverslips were treated sequentially with 0.2% gelatin (Sigma-Aldrich), 1% glutaraldehyde (Electron Microscopy Sciences, Hatfield, PA, USA), and 1 M ethanolamine (Sigma-Aldrich). The RF/6A ECs plated on the cross-linked cover slips were subjected to SS treatment for 10 days, followed by overnight decellularization of the endothelial monolayer with 20 mM ammonium hydroxide (Sigma-Aldrich) and 0.5% Triton X-100 (Sigma-Aldrich) in Ca^{2+}, Mg^{2+}-free $PBS^{-/-}$ (Life Technologies). Next, the decellularized BM samples were treated with 7.5 KU units of DNase (Qiagen, Venlo, The Netherlands) in distilled H_2O followed by washing with Ca^{2+}, Mg^{2+}-containing $PBS^{+/+}$. The decellularized BM then were fixed with 1% paraformaldehyde (PFA; Electron Microscopy Sciences) followed by labeling with rabbit anti-collagen IV (Abcam, Cambridge, UK) and fluorescein conjugated goat anti-rabbit IgG secondary antibody (Life Technologies). Fluorescent xyz- and xzy-plane images of the immunolabeled BM were acquired with a Leica SP5 inverted confocal microscope (Leica Camera AG, Solms, Germany). BM thickness (three replicates per condition) was analyzed using ImageJ software (National Institutes of Health [NIH], Bethesda, MD, USA).

Cell Viability Assay

To measure cell viability, RF/6A ECs were plated in 96-well plates and grown in medium containing varying doses of SS for 10 days. Cell viability was determined in these 10-day SS-treated cultures using XTT Cell Viability Assay Kit (Biotium, Hayward, CA, USA), as per the manufacturer's protocol. To evaluate the effect of SS-treated BM on cell viability, normal (non–SS-treated) ECs were plated on decellularized SS-treated BM samples in SS-free or SS-containing complete growth medium. Cell viability (four replicates per condition) was normalized with respect to the non–SS-treated control.

Cell Spreading and Cytoskeletal Organization

To evaluate cell spreading, RF/6A ECs were grown in medium containing varying SS doses for 10 days. The SS-treated confluent cells then were detached and replated on fresh cover slips at 15,000 cells/cm^2 in medium containing the corresponding SS doses. Six hours after plating, cells were fixed with 1% PFA, permeabilized with 0.2% Triton X-100, and stained with Alexa Fluor-488 phalloidin and DAPI for visualization of actin microfilaments and nuclei, respectively. Phase images (×20) and fluorescence images (×60) were acquired with a Nikon Eclipse TI fluorescence microscope fitted with a Nikon Digital Sight DS-QiMc camera (Nikon Corporation, Tokyo, Japan). Cell area and the number of actin filaments were quantified using ImageJ software (NIH). At least 40 cells were analyzed for spreading and at least 20 cells for actin filament density. To determine the effect of SS-treated BM on cell spreading and actin cytoskeletal organization, normal (non–SS-treated) ECs were plated on decellularized SS-treated BM samples in SS-free or SS-containing complete growth

Investigative Ophthalmology & Visual Science

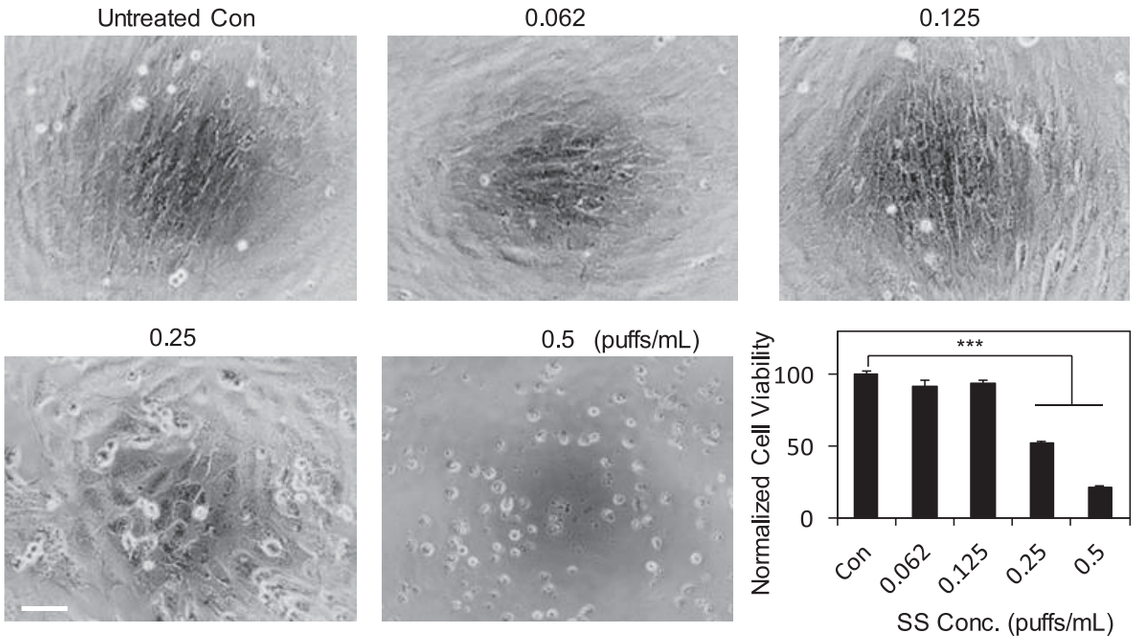

Figure 1. Exposure to SS causes choroidal EC monolayer retraction and loss of cell viability. Phase contrast images of RF/6A EC monolayer treated with SS for 10 days show progressively greater monolayer retraction at higher SS doses, with 0.5 puffs/mL causing the greatest disruption. This SS-induced EC monolayer retraction correlates with a significant decrease in EC viability, as shown in the bar graph. Data are presented as percentage cells that are viable with respect to the non–SS-treated control. $^{***}P < 0.001$. *Scale bar*: 100 μm.

medium. Cell area and actin filament density were quantified as described above.

LOX Expression

Lysyl oxidase expression in SS-treated RF/6A ECs was determined by Western blot. Briefly, 10-day SS-treated confluent cells were lysed in RIPA buffer containing protease and phosphatase inhibitors, and the lysates were centrifuged to obtain protein supernatant. An equal amount of protein was loaded in 10% SDS–polyacrylamide gel and the separated proteins transferred onto a nitrocellulose membrane for detection with polyclonal rabbit anti-LOX antibody (Novus Biologicals, Littleton, CO, USA) and horseradish peroxidase (HRP)–conjugated secondary antibody (Vector Laboratories, Inc., Burlingame, CA, USA). Glyceraldehyde-3-phosphate dehydrogenase (GAPDH) was used as the loading control. A chemiluminescent detection kit (Thermo Scientific, Rockford, IL, USA) was used to visualize the bands, and ImageJ software was used to perform densitometric analysis.

Statistics

All data were obtained from multiple replicates, as indicated in the respective procedures, and expressed as mean ± SEM. Statistical significance was determined using ANOVA, followed by Tukey and Bonferroni post hoc analysis (Instat; GraphPad Software, Inc., San Diego, CA, USA). Results were considered significant if $P < 0.05$.

Results

SS Exposure Causes Choroidal EC Monolayer Retraction and Loss of Cell Viability

To determine whether SS contributes to choriocapillaris dysfunction, RF/6A EC monolayers were treated with varying doses of SS and cell viability measured after 10 days of treatment. Our liquid chromatography-tandem mass spectrometry measurements confirmed that these SS working solutions contain nicotine in a range similar to that found in tissues following exposure to SS (approximately 35–350 ng/ml[29–31]). Specifically, nicotine concentrations in the final SS working doses were found to be 144.2 ng/mL (corresponding to 0.062 puffs/mL), 290.7 ng/mL (0.125 puffs/mL), and 581.4 ng/mL (0.25 puffs/mL).

Phase images of SS-treated cells revealed partial or complete retraction of the monolayer at doses of 0.25 or 0.5 puffs/mL, respectively (Fig. 1), reminiscent of endothelium disruption in choriocapillaris observed during early AMD.[6] We next looked to see whether this monolayer retraction at higher SS doses correlates with decreased EC viability. Quantitative measurement of cell viability with the XTT assay indicated a dose-dependent inhibitory effect of SS, with the higher doses of 0.25 and 0.5 puffs/mL causing significant inhibition (48% and 79% inhibition with 0.25 and 0.5 puffs/mL, respectively; $P < 0.001$) of EC viability when compared to the non–SS-treated control. Endothelial cells treated with mainstream smoke, however, exhibited no significant decrease in cell viability or increase in cell retraction (Supplementary Fig. S1), confirming previous reports that SS exerts significantly greater cytotoxic effects than mainstream smoke.[32,33]

Choroidal EC Spreading and Cytoskeletal Organization Are Impaired by SS

Endothelial cell life, death, and function are known to be mediated strongly by actin cytoskeleton-dependent cell shape.[11,12,19] Therefore, we asked whether the SS-dependent inhibition of RF/6A EC viability resulted from impairment of these physical determinants. To quantify the effects of SS treatment on EC spreading, we measured the projected cell area of individual ECs. As shown in the phase images and quantified in the bar graph (Fig. 2A), cell spreading decreased

Investigative Ophthalmology & Visual Science

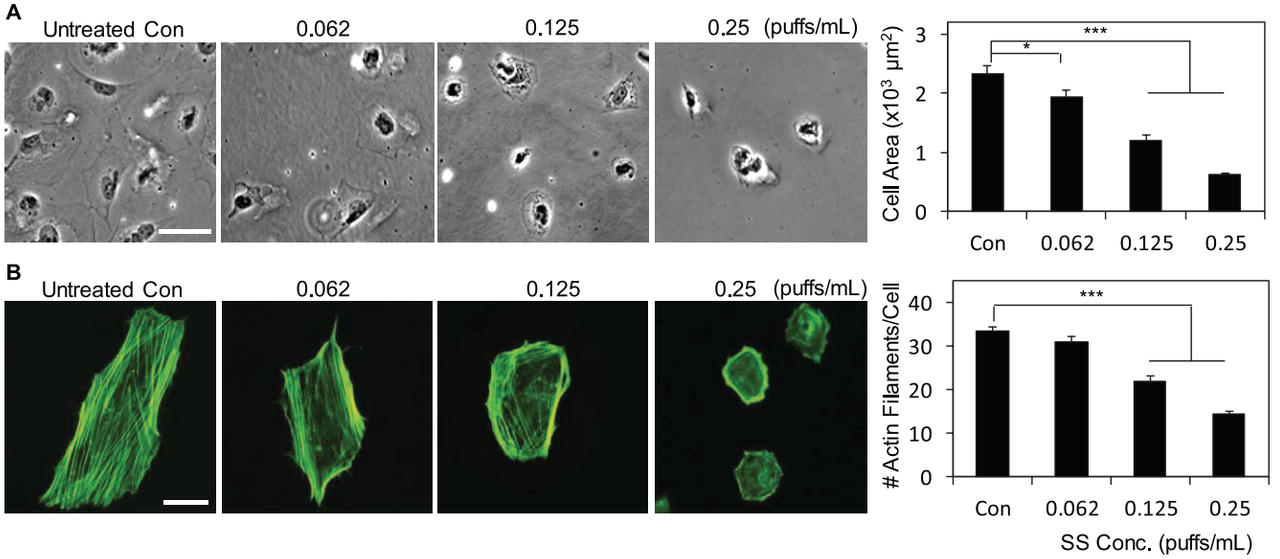

FIGURE 2. Choroidal EC spreading and cytoskeletal organization are impaired by SS. (**A**) Phase contrast images of RF/6A ECs and measurement of projected cell area (bar graph) reveal a dose-dependent decrease in EC spreading upon SS treatment. *Scale bar*: 100 μm. (**B**) Fluorescent images of ECs stained with phalloidin show that the longitudinal orientation of actin stress fibers in untreated ECs changes to cortical organization in SS-treated ECs. Morphometric analysis further revealed a progressive decrease in actin filament density with increasing SS dose (bar graph). $^{*}P < 0.05$ and $^{***}P < 0.001$, respectively. *Scale bar*: 20 μm.

significantly with increasing SS dose. Specifically, when compared with the non–SS-treated condition, SS doses of 0.062, 0.125, and 0.25 puffs/mL caused a 15% ($P < 0.05$), 49%, and 74% (both $P < 0.001$) reduction in cell area, respectively. To determine whether this inhibition of EC spreading resulted from disruption of the cell's actin cytoskeletal density/organization, we labeled these cells with phalloidin, which selectively stains actin filaments. As shown in the fluorescent images and quantified in the bar graph (Fig. 2B), the significant SS-mediated decrease in cell spreading correlated strongly with a concomitant decrease in actin filament density, with SS doses of 0.125 and 0.25 puffs/mL causing a 35% and 58% (both $P < 0.001$) reduction in actin filament density, respectively, when compared to untreated control ECs. In addition to their density, the organization of actin filaments was also markedly altered in response to SS where the longitudinal actin stress fibers in untreated ECs were gradually replaced by a cortical actin network in SS-treated ECs. This alteration in actin organization is known to be a consequence of cell rounding.[34,35]

SS Exposure Disrupts Choroidal Endothelial BM Organization Through Suppression of LOX-Mediated Crosslinking

Variations in ECM structure can significantly alter cell shape-dependent vascular endothelial function.[12,36,37] Thus, we looked to see whether the SS-induced impairment of RF/6A EC architecture and viability resulted from aberrant structure of the underlying BM. The EC-derived BM was obtained by decellularizing the EC monolayer after 10 days of SS treatment and visualized by immunofluorescent staining for collagen IV, the predominant structural protein of endothelial BM. Confocal imaging of collagen IV in XY plane showed a dose-dependent disruption of basement membrane organization (Fig. 3), with the BM density decreasing and pore size increasing with increasing SS dose. To quantify these changes, we took XZ plane images and measured the thickness of deposited BM. Consistent with the trend seen in XY planar images, increasing SS dose caused progressive basement membrane thinning. Specifically, when compared to non–SS-treated condition, SS doses of 0.062, 0.125, and 0.25 puffs/mL caused a 29%, 56%, and 65% (all $P < 0.001$) reduction in BM thickness, respectively.

Lysyl oxidase is a copper-dependent enzyme that covalently crosslinks collagen that has a key role in ECM organization.[21] Indeed, suppression of LOX expression leads to ECM structural defects and vascular dysfunction.[37] Thus, we hypothesized that SS-induced disruption of RF/6A EC-derived BM likely results from suppression of LOX expression by these cells. Western blot analysis of SS-treated ECs confirmed this hypothesis where the SS dose of 0.062 puffs/mL led to a significant ($P < 0.001$) 15% decrease in LOX expression, 0.125 puffs/mL caused a 44% reduction, while 0.25 puffs/mL caused a 52% inhibition in LOX expression (Fig. 4).

Active Role of SS-Treated BM in EC Dysfunction

Since SS was found to disrupt BM architecture, we asked whether the SS-treated corrupt endothelial BM can, in turn, feed back to impair RF/6A EC form and behavior. To address this question, we plated non–SS-treated ECs on decellularized SS-treated BM and monitored cell shape, actin cytoskeletal organization, and viability (Fig. 5A). Phalloidin staining and subsequent image analysis revealed that both actin filament density (Figs. 5B, 5C) and spreading (Fig. 5D) of freshly-plated ECs decreased progressively on BMs treated with higher SS doses. Specifically, when compared to non–SS-treated BM condition, ECs plated on BMs treated with SS doses of 0.062, 0.125, and 0.25 puffs/mL underwent an 8% (not significant, $P > 0.05$), 17% ($P < 0.01$), and 42% ($P < 0.001$) reduction in actin filament density, and a 23%, 36%, and 49% (all $P < 0.001$) reduction in cell area, respectively. Further, the organization of actin filaments was also markedly altered in cells grown on SS-treated BM, which assumed a distinct cortical actin network in contrast to the longitudinal actin stress fibers on non–SS-treated BM (Fig. 5B). Consistent with the disruption in cell shape and actin cytoskeletal organization, cell viability was also impaired on these aberrant SS-treated BM (Fig. 5E), thereby

Investigative Ophthalmology & Visual Science

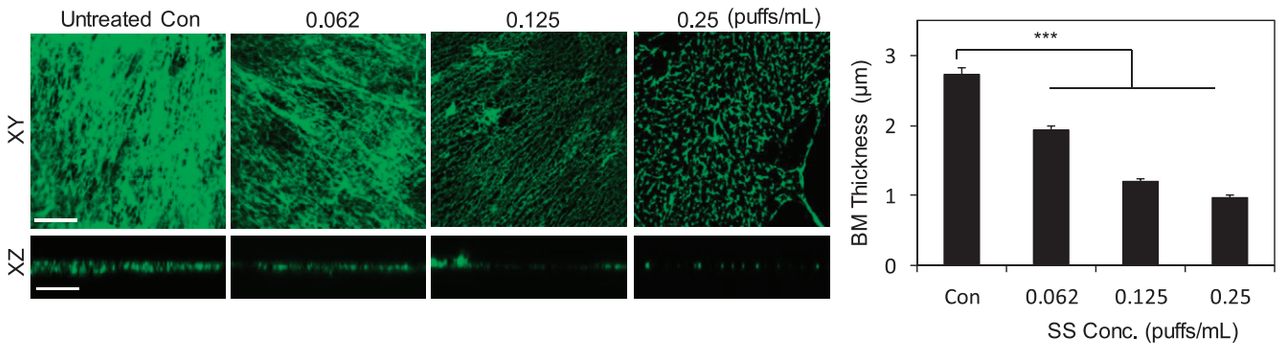

Figure 3. Exposure to SS disrupts choroidal endothelial BM architecture. *Top view* (XY plane) of RF/6A EC-secreted collagen IV network shows that, compared to untreated ECs, those treated with SS exhibit a dose-dependent decrease in BM density and a concomitant increase in BM porosity. These alterations in BM organization correlate with significant (***$P < 0.001$) BM thinning at higher SS doses, as shown in the cross-sectional (XZ plane) view and quantified in the bar graph. *Scale bars*: 10 μm (XY image); 5 μm (XZ image).

underscoring the key role that BM organization has in cell shape- and cytoskeleton-dependent control of cell behavior.

To further emphasize the critical role of corrupt SS-treated BM in impaired RF/6A architecture and viability, we performed two additional experiments. Firstly, we plated cells on regular (non–SS-treated) surface in SS-containing medium. Under this condition, cell spreading was found to be similar across the different SS doses (Supplementary Fig. S2). Secondly, we did the converse experiment, where we plated cells on SS-treated BM in SS-free medium. Under this condition, where no SS was present in the medium, the disruption in cell spreading, cytoskeletal organization, and viability still was significant (Supplementary Fig. S3). Thus, taken together, these studies indicated that the corrupt SS-treated BM contributes significantly to the inhibition in RF/6A viability seen with SS treatment.

Discussion

Although ETS long has been considered a major risk factor for AMD, its precise role in disease initiation and progression remains poorly understood. The implication of vascular dysfunction in AMD has been examined conventionally in the context of angiogenic and leaky choroidal vessels that arise during late-stage wet AMD. However, new studies indicate that defects in choriocapillaris, characterized by EC loss, also occur early on during the onset of drusen formation.[6] The goal of this work was to advance our understanding of AMD pathophysiology by determining how SS, the major component of ETS, contributes to this early-stage choroidal vascular dysfunction. Our findings demonstrate that SS exposure causes significant dose-dependent retraction of choroidal EC monolayer and inhibition of EC viability, which are key determinants of choroidal vessel form and function. Further, this decrease in SS-induced choroidal endothelial viability was found to result, at least in part, from the abnormal architecture of the cell cytoskeleton and the underlying BM.

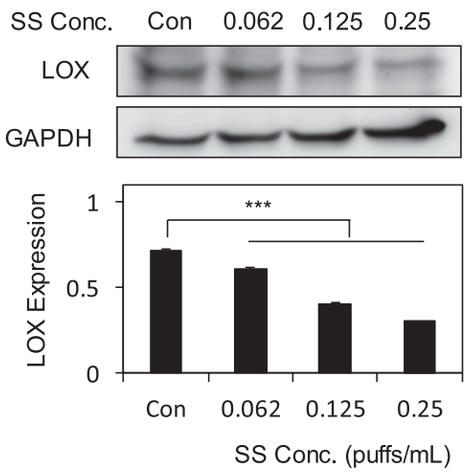

Figure 4. Exposure to SS suppresses LOX expression by choroidal ECs. Western blot bands and their densitometric analyses (bar graph) together reveal that LOX expression by RF/6A ECs decreases progressively with increasing SS dose. The LOX levels were normalized with respect to the corresponding levels of GAPDH, which served as the loading control. ***$P < 0.001$.

Tobacco smoke is a systemic toxicant that affects the vasculature of various tissues and organs in the body, thus contributing to myriad pathologic conditions. For instance, past studies have shown that tobacco smoke exposure causes impairment of lung EC signaling,[38] and apoptosis,[39] which are strongly implicated in tobacco-induced lung emphysema. Tobacco smoke is also known to be a potent cardiovascular risk factor, with tobacco-induced arterial/aortic endothelial dysfunction being a critical determinant.[40–42] Tobacco smoke can also impair the survival and growth of skin-derived ECs,[43] and disrupt neovascularization in embryonic tissues.[44] These reports of tobacco smoke–induced systemic endothelial defects are consistent with increased levels of plasma von Willebrand factor (vWF), a marker for endothelial dysfunction.[45] The current study presents the first evidence that SS exposure also causes significant choroidal vascular dysfunction, which manifests as lower EC viability and greater endothelial monolayer retraction. Together, these tobacco smoke–induced endothelial defects may contribute to the choroidal EC loss, occurrence of "ghost" vessels, and vascular collapse seen in the early-stage (dry) AMD.[6]

To understand exactly how SS disrupts choroidal endothelial viability and monolayer integrity, we examined its effect on cell shape and cytoskeletal architecture, physical cues that alone can regulate EC death, proliferation, and capillary formation.[11,12] Specifically, cell rounding and actin cytoskeleton disassembly leads to apoptosis, maximal cell spreading with robust actin cytoskeleton promotes proliferation, while partial cell retraction due to an increase in actin cytoskeleton-dependent contractility spontaneously initiates three-dimensional capillary formation. The actin cytoskeleton also orients much of the intracellular biochemistry,[46] which may explain its pivotal role in regulating cell fate. Our finding that SS-mediated

Investigative Ophthalmology & Visual Science

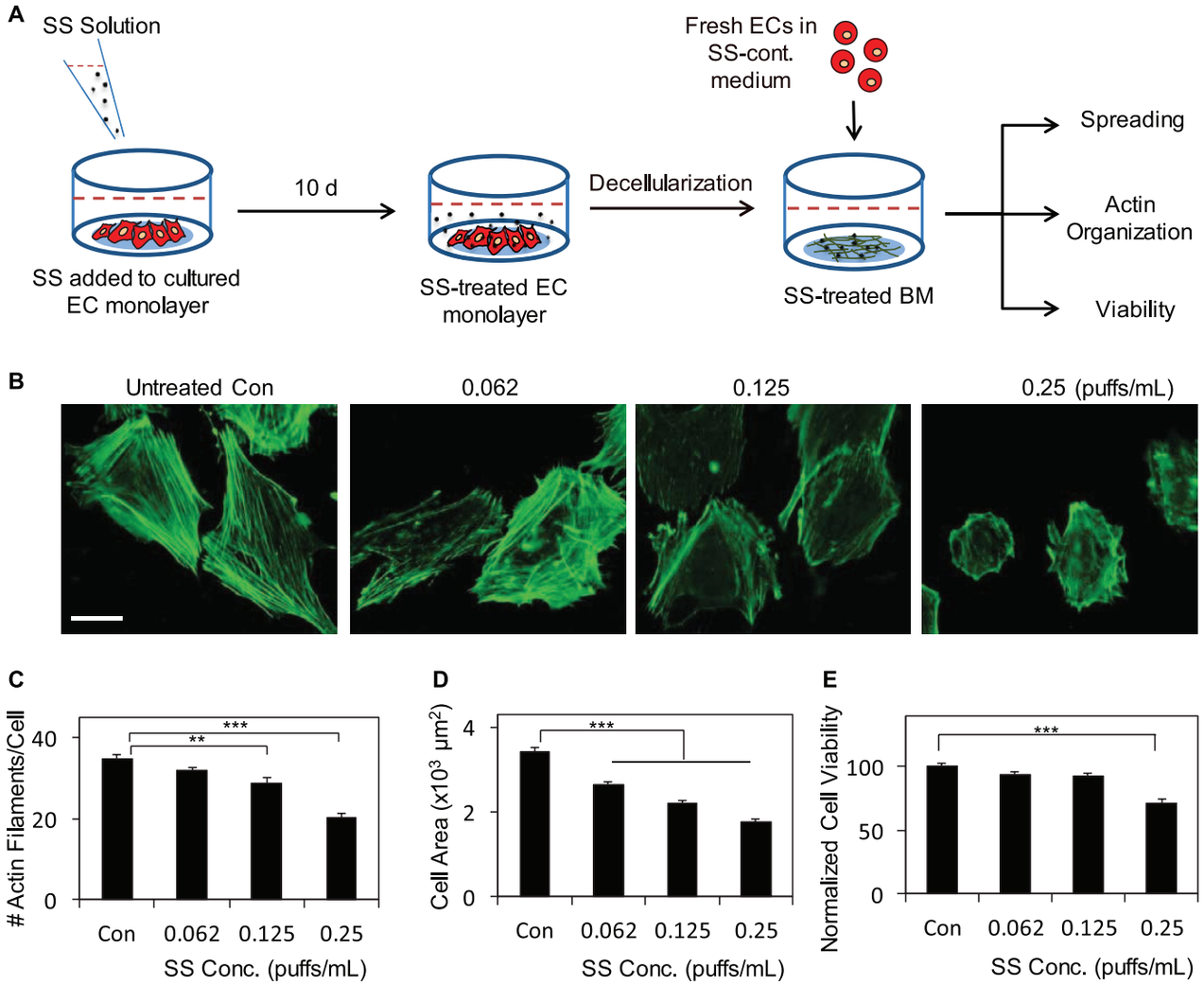

Figure 5. The SS-treated corrupt BM alone can disrupt EC cytoskeletal organization, spreading, and viability. (**A**) Schematic depiction of the experimental procedure to examine the effect of SS-treated corrupt BM on untreated RF/6A ECs. (**B**) Fluorescent images of ECs stained with phalloidin show that ECs cultured on untreated BM exhibit longitudinal orientation of actin stress fibers, while those grown on SS-treated corrupt BM undergo cortical actin assembly. Morphometric analysis further revealed a progressive decrease in actin filament density with increasing SS dose (**C**), which correlated well with decreased EC spreading (**D**) and viability (**E**) on SS-treated corrupt BM. The EC viability data are presented as percentage cells that are viable with respect to non–SS-treated BM control. $^{**}P < 0.01$ and $^{***}P < 0.001$, respectively. *Scale bar*: 20 μm.

inhibition of cell viability occurs concomitantly with a significant disruption in choroidal EC spreading and actin cytoskeletal organization further emphasizes the physical basis of SS-induced choroidal endothelial dysfunction. Notably, since SS-induced RF/6A cell retraction is caused by disruption of actin cytoskeleton, and thus by a likely decrease in cell contractility, the partially retracted RF/6A cells undergo loss of viability instead of spontaneous capillary formation. This physical view of tobacco smoke–induced vascular dysfunction is supported further by a past study where aortic endothelial cells treated with nicotine, a major toxicant in SS, underwent cell retraction through disruption of endothelial actin stress fibers and simultaneous organization of cortical actin,[47] as observed here in SS-treated RF/6A cells.

The physical control of vascular endothelial fate also depends critically on the mechanostructural properties of the underlying ECM, which helps establish a cell-ECM force balance that mediates endothelial mechanotransduction.[20,46] Indeed, abnormal basement membrane thinning or thickening has been implicated in endothelial dysfunction and vascular anomalies characteristic of various pathologies, such as cancer, atherosclerosis, and hypertension.[18,20,48] Our findings that (1) SS causes thinning of choroidal endothelial BM, and (2) fresh ECs plated on SS-modified BM exhibit impaired cell spreading and viability implicate extracellular physical cues as an important determinant of choriocapillaris defects in tobacco smoke–associated AMD. Tobacco-induced BM breakdown/thinning and endothelial loss are also seen in emphysematous lung alveolar capillaries,[49,50] which further implicates aberrant BM structure as an important determinant of tobacco smoke–induced choroidal endothelial dysfunction.

We further show that the disruption of collagen IV BM by SS correlates strongly with impaired expression of LOX, a copper-dependent amine oxidase that crosslinks collagen through deamination of lysine and hydroxylysine residues.[21] Lysyl oxidase and other LOX-like proteins (LOXL 1–4) provide vital

structural stability to vascular basement membrane, and impairment in their expression/activity leads to severe vascular collapse and dysfunction.[17,37,51] Notably, tobacco exposure markedly suppresses LOX expression by lung fibroblasts.[52] Thus, together with these past findings, our new evidence implicates endothelial LOX as a key mediator of BM-dependent choroidal endothelial dysfunction in response to SS.

It is important to point out that, although there is substantial epidemiologic evidence of a strong correlation between tobacco smoke and incidence of AMD,[1,2] the direct causal relationship between SS exposure and drusen formation has not yet been demonstrated. To our knowledge, the findings described here that link SS exposure to choroidal EC dysfunction represent the first step in examining this relationship as loss of choriocapillaris has been previously implicated in drusen formation.[6] However, more detailed in vitro and in vivo studies will need to be performed in the future to determine whether and how SS-mediated loss of choroidal vessels is causally linked to dry AMD. It is also important to note that not all tobacco-smoking individuals develop AMD symptoms, which may be attributed to the fact that the risk of drusen formation is also influenced strongly by the presence of some susceptibility genes, in particular *ARMS2* and *HTRA1*, that undergo polymorphisms in individuals with AMD.[53] Thus, tobacco-smoking individuals with aberrant *ARMS2* and *HTRA1* genes will have a markedly higher probability of developing drusen than those with normal genotype.

Since choroidal vessels are the major source of oxygen and nutrient exchange for the overlying RPE, disruption of choriocapillaris by SS also may cause RPE hypoxic stress and dysfunction, a major causative factor for AMD. However, as recent studies have shown, SS exposure also may directly disrupt RPE. For instance, treatment of RPE culture with nicotine, the most commonly investigated SS toxicant, caused cell thinning/flattening and dissolution of actin cytoskeleton, while nicotine-fed mice exhibited damaged photoreceptor-RPE interface.[54] Further, treatment of RPE culture with benzo(e)-pyrene, a carcinogenic chemical found commonly in SS,[33] produced a dose-dependent reduction in cell viability, while significantly increasing the apoptotic pathway.[55] Thus, given that SS exposure may simultaneously affect the choriocapillaris and RPE, experimental models that can examine this choriocapillaris/RPE interface will provide truly important insights into SS-induced AMD pathogenesis.

In summary, we here examined the pathophysiology of SS-induced choroidal vascular dysfunction that is characteristic of dry AMD and found that SS exposure causes choroidal endothelial monolayer regression that results, at least in part, from disruption of cell shape/cytoskeleton-dependent cell viability. We further showed that impaired expression of LOX and the subsequent breakdown of endothelial BM likely mediate these detrimental effects of SS on choroidal ECs. By highlighting the crucial role that physical cues have in choroidal vascular dysfunction, this study provided new mechanistic insights into the pathophysiology of degenerative AMD. Future studies that uncover the various cellular and extracellular mediators of this physical control of choroidal endothelial dysfunction may lead to the development of an entirely new class of AMD therapeutics.

Acknowledgments

The authors thank Irit Adini for helpful comments on the manuscript.

Supported by Initial Complement Funds provided by the University of California-Riverside Bourns College of Engineering.

Disclosure: **X. Yang**, None; **H.A. Scott**, None; **S. Ardekani**, None; **M. Williams**, None; **P. Talbot**, None; **K. Ghosh**, None

References

1. Thornton J, Edwards R, Mitchell P, Harrison RA, Buchan I, Kelly SP. Smoking and age-related macular degeneration: a review of association. *Eye (Lond)*. 2005;19:935–944.
2. Evans JR, Fletcher AE, Wormald RP. 28,000 Cases of age related macular degeneration causing visual loss in people aged 75 years and above in the United Kingdom may be attributable to smoking. *Br J Ophthalmol*. 2005;89:550–553.
3. Ambati J, Fowler BJ. Mechanisms of age-related macular degeneration. *Neuron*. 2012;75:26–39.
4. Kaiser PK. Emerging therapies for neovascular age-related macular degeneration: drugs in the pipeline. *Ophthalmology*. 2013;120:S11–S15.
5. Stone EM. A very effective treatment for neovascular macular degeneration. *N Engl J Med*. 2006;355:1493–1495.
6. Mullins RF, Johnson MN, Faidley EA, Skeie JM, Huang J. Choriocapillaris vascular dropout related to density of drusen in human eyes with early age-related macular degeneration. *Invest Ophthalmol Vis Sci*. 2011;52:1606–1612.
7. Skeie JM, Fingert JH, Russell SR, Stone EM, Mullins RF. Complement component C5a activates ICAM-1 expression on human choroidal endothelial cells. *Invest Ophthalmol Vis Sci*. 2010;51:5336–5342.
8. McLeod DS, Grebe R, Bhutto I, Merges C, Baba T, Lutty GA. Relationship between RPE and choriocapillaris in age-related macular degeneration. *Invest Ophthalmol Vis Sci*. 2009;50:4982–4991.
9. Jarrett SG, Boulton ME. Consequences of oxidative stress in age-related macular degeneration. *Mol Aspects Med*. 2012;33:399–417.
10. Cai X, McGinnis JF. Oxidative stress: the Achilles' heel of neurodegenerative diseases of the retina. *Front Biosci (Landmark Ed)*. 2012;17:1976–1995.
11. Dike LE, Chen CS, Mrksich M, Tien J, Whitesides GM, Ingber DE. Geometric control of switching between growth, apoptosis, and differentiation during angiogenesis using micropatterned substrates. *In Vitro Cell Dev Biol Anim*. 1999;35:441–448.
12. Ingber DE. Mechanical signaling and the cellular response to extracellular matrix in angiogenesis and cardiovascular physiology. *Circ Res*. 2002;91:877–887.
13. Davis GE, Senger DR. Endothelial extracellular matrix: biosynthesis, remodeling, and functions during vascular morphogenesis and neovessel stabilization. *Circ Res*. 2005;97:1093–1107.
14. Ghosh K, Thodeti CK, Dudley AC, Mammoto A, Klagsbrun M, Ingber DE. Tumor-derived endothelial cells exhibit aberrant Rho-mediated mechanosensing and abnormal angiogenesis in vitro. *Proc Natl Acad Sci U S A*. 2008;105:11305–11310.
15. Wang N, Tytell JD, Ingber DE. Mechanotransduction at a distance: mechanically coupling the extracellular matrix with the nucleus. *Nat Rev Mol Cell Biol*. 2009;10:75–82.
16. Mammoto A, Mammoto T, Ingber DE. Mechanosensitive mechanisms in transcriptional regulation. *J Cell Sci*. 2012;125:3061–3073.
17. Bignon M, Pichol-Thievend C, Hardouin J, et al. Lysyl oxidase-like protein-2 regulates sprouting angiogenesis and type IV collagen assembly in the endothelial basement membrane. *Blood*. 2011;118:3979–3989.
18. Sund M, Xie L, Kalluri R. The contribution of vascular basement membranes and extracellular matrix to the mechanics of tumor angiogenesis. *APMIS*. 2004;112:450–462.

Investigative Ophthalmology & Visual Science

19. van Nieuw Amerongen GP, Koolwijk P, Versteilen A, van Hinsbergh VW. Involvement of RhoA/Rho kinase signaling in VEGF-induced endothelial cell migration and angiogenesis in vitro. *Arterioscler Thromb Vasc Biol*. 2003;23:211–217.
20. Hahn C, Schwartz MA. Mechanotransduction in vascular physiology and atherogenesis. *Nat Rev Mol Cell Biol*. 2009; 10:53–62.
21. Kagan HM, Li W. Lysyl oxidase: properties, specificity, and biological roles inside and outside of the cell. *J Cell Biochem*. 2003;88:660–672.
22. Melkonian G, Cheung L, Marr R, Tong C, Talbot P. Mainstream and sidestream cigarette smoke inhibit growth and angiogenesis in the day 5 chick chorioallantoic membrane. *Toxicol Sci*. 2002;68:237–248.
23. Knoll M, Talbot P. Cigarette smoke inhibits oocyte cumulus complex pick-up by the oviduct in vitro independent of ciliary beat frequency. *Reprod Toxicol*. 1998;12:57–68.
24. Hahn EJ, Rayens MK, York N, et al. Effects of a smoke-free law on hair nicotine and respiratory symptoms of restaurant and bar workers. *J Occup Environ Med*. 2006;48:906–913.
25. Bates MN, Fawcett J, Dickson S, Berezowski R, Garrett N. Exposure of hospitality workers to environmental tobacco smoke. *Tob Control*. 2002;11:125–129.
26. EPA. Respiratory health effects of passive smoking: lung cancer and other disorders. *EPA Report/600/6-90/006F*. Washington, DC: EPA; 1992.
27. Beacham DA, Amatangelo MD, Cukierman E. Preparation of extracellular matrices produced by cultured and primary fibroblasts. *Curr Protoc Cell Biol*. 2007;Chapter 10:Unit 10.9.
28. Bischof AG, Yuksel D, Mammoto T, Mammoto A, Krause S, Ingber DE. Breast cancer normalization induced by embryonic mesenchyme is mediated by extracellular matrix biglycan. *Integr Biol (Camb)*. 2013;5:1045–1056.
29. Leeds J, Turner DM. Factors affecting the tissue binding of nicotine in various species. *Biochem Pharmacol*. 1977;26: 1631–1635.
30. Adir J, Miller RP, Rotenberg KS. Disposition of nicotine in the rat after intravenous administration. *Res Commun Chem Pathol Pharmacol*. 1976;13:173–183.
31. Yamamoto I, Inkoi R, Iwatsubo K. Penetration of nicotine-^{14}C into several rat tissues in vivo and in vitro. *Toxicol Appl Pharmacol*. 1968;12:560–567.
32. Schick S, Glantz S. Philip Morris toxicological experiments with fresh sidestream smoke: more toxic than mainstream smoke. *Tob Control*. 2005;14:396–404.
33. Schick S, Glantz S. Scientific analysis of second-hand smoke by the tobacco industry, 1929-1972. *Nicotine Tob Res*. 2005;7: 591–612.
34. Maddox AS, Burridge K. RhoA is required for cortical retraction and rigidity during mitotic cell rounding. *J Cell Biol*. 2003;160:255–265.
35. Ren XD, Kiosses WB, Schwartz MA. Regulation of the small GTP-binding protein Rho by cell adhesion and the cytoskeleton. *EMBO J*. 1999;18:578–585.
36. Ghosh K, Ingber DE. Micromechanical control of cell and tissue development: implications for tissue engineering. *Adv Drug Deliv Rev*. 2007;59:1306–1318.
37. Mammoto A, Mammoto T, Kanapathipillai M, et al. Control of lung vascular permeability and endotoxin-induced pulmonary oedema by changes in extracellular matrix mechanics. *Nat Commun*. 2013;4:1759.
38. Edirisinghe I, Arunachalam G, Wong C, et al. Cigarette-smoke-induced oxidative/nitrosative stress impairs VEGF- and fluid-shear-stress-mediated signaling in endothelial cells. *Antioxid Redox Signal*. 2010;12:1355–1369.
39. Green LA, Petrusca D, Rajashekhar G, et al. Cigarette smoke-induced CXCR3 receptor up-regulation mediates endothelial apoptosis. *Am J Respir Cell Mol Biol*. 2012;47:807–814.
40. Bernhard D, Rossmann A, Henderson B, Kind M, Seubert A, Wick G. Increased serum cadmium and strontium levels in young smokers: effects on arterial endothelial cell gene transcription. *Arterioscler Thromb Vasc Biol*. 2006;26:833–838.
41. Peluffo G, Calcerrada P, Piacenza L, Pizzano N, Radi R. Superoxide-mediated inactivation of nitric oxide and peroxynitrite formation by tobacco smoke in vascular endothelium: studies in cultured cells and smokers. *Am J Physiol Heart Circ Physiol*. 2009;296:H1781–H1792.
42. Breitling LP. Current genetics and epigenetics of smoking/tobacco-related cardiovascular disease. *Arterioscler Thromb Vasc Biol*. 2013;33:1468–1472.
43. Yu R, Wu M, Lin S, Talbot P. Cigarette smoke toxicants alter growth and survival of cultured mammalian cells. *Toxicol Sci*. 2006;93:82–95.
44. Melkonian G, Le C, Zheng W, Talbot P, Martins-Green M. Normal patterns of angiogenesis and extracellular matrix deposition in chick chorioallantoic membranes are disrupted by mainstream and sidestream cigarette smoke. *Toxicol Appl Pharmacol*. 2000;163:26–37.
45. Lip PL, Blann AD, Hope-Ross M, Gibson JM, Lip GY. Age-related macular degeneration is associated with increased vascular endothelial growth factor, hemorheology and endothelial dysfunction. *Ophthalmology*. 2001;108:705–710.
46. Ingber DE. Tensegrity II. How structural networks influence cellular information processing networks. *J Cell Sci*. 2003;116: 1397–1408.
47. Cucina A, Sapienza P, Borrelli V, et al. Nicotine reorganizes cytoskeleton of vascular endothelial cell through platelet-derived growth factor BB. *J Surg Res*. 2000;92:233–238.
48. Ingber DE. Mechanobiology and diseases of mechanotransduction. *Ann Med*. 2003;35:564–577.
49. Salazar LM, Herrera AM. Fibrotic response of tissue remodeling in COPD. *Lung*. 2011;189:101–109.
50. Kasahara Y, Tuder RM, Taraseviciene-Stewart L, et al. Inhibition of VEGF receptors causes lung cell apoptosis and emphysema. *J Clin Invest*. 2000;106:1311–1319.
51. Levene CI, Heale G, Robins SP. Collagen cross-link synthesis in cultured vascular endothelium. *Br J Exp Pathol*. 1989;70:621–626.
52. Gao S, Chen K, Zhao Y, et al. Transcriptional and posttranscriptional inhibition of lysyl oxidase expression by cigarette smoke condensate in cultured rat fetal lung fibroblasts. *Toxicol Sci*. 2005;87:197–203.
53. Francis PJ, Appukuttan B, Simmons E, et al. Rhesus monkeys and humans share common susceptibility genes for age-related macular disease. *Hum Mol Genet*. 2008;17:2673–2680.
54. Yang L, Gong H, Wang Y, Yin H, Chen P, Zhang H. Nicotine alters morphology and function of retinal pigment epithelial cells in mice. *Toxicol Pathol*. 2010;38:560–567.
55. Sharma A, Neekhra A, Gramajo AL, et al. Effects of Benzo(e)Pyrene, a toxic component of cigarette smoke, on human retinal pigment epithelial cells in vitro. *Invest Ophthalmol Vis Sci*. 2008;49:5111–5117.

Investigative Ophthalmology & Visual Science